ACCSCIENCE PUBLISHING

International Journal of Bioprinting

RESEARCH ARTICLE

3D-printed nano-hydroxyapatite/polylactic acid scaffold with simvastatin-loaded hydroxyethyl methacrylate/sulfobetaine methacrylate hydrogel for accelerated bone repair

Yang Qu[1,2†], Ya-nan Wang[3†], Weiqing Kong[4], Xiaofan Du[1], Jianyi Li[1], Yukun Du[1], Guanghui Gu[1*], and Yongming Xi[1*]

[1]Department of Spinal Surgery, The Affiliated Hospital of Qingdao University, Qingdao, Shandong, China

[2]Key Laboratory of Trauma and Neural Regeneration, Ministry of Education and National Center for Trauma Medicine, Department of Orthopedics and Trauma, Peking University People's Hospital, Beijing, China

[3]Department of Nuclear Medicine, Xuzhou Central Hospital, Southeast University, Xuzhou, Jiangsu, China

[4]Department of Orthopedics, Xuzhou Central Hospital, Southeast University, Xuzhou, Jiangsu, China

[†]These authors contributed equally to this work.

***Corresponding authors:**
Guanghui Gu
(guguanghui@qdu.edu.cn)

Yongming Xi
(xym700118@qdu.edu.cn)

Citation: Qu Y, Wang Y, Kong W, *et al.* 3D-printed nano-hydroxyapatite/polylactic acid scaffold with simvastatin-loaded hydroxyethyl methacrylate/sulfobetaine methacrylate hydrogel for accelerated bone repair. *Int J Bioprint.* 2026;12(1):656-671. doi: 10.36922/IJB025490505

Received: December 2, 2025
Revised: January 1, 2026
Accepted: January 1, 2026
Published Online: January 14, 2026

Abstract

Bone defects resulting from trauma, infection, or tumor resection often exceed the self-healing capacity of bone tissue, requiring bioactive and mechanically robust repair materials. In this study, a composite scaffold was developed via *in situ* polymerization of a hydroxyethyl methacrylate/sulfobetaine methacrylate (HMSM) hydrogel with a three-dimensional-printed nano-hydroxyapatite/polylactic acid (NP) gradient scaffold to achieve controlled simvastatin (SIM) delivery and enhanced osteogenesis. The HMSM hydrogel served as a hydrophilic and biocompatible matrix, while the NP scaffold provided mechanical strength and structural support. SIM was incorporated into the hydrogel–scaffold composite (SIM@HMSM/NP) to establish a sustained drug-release system. The composite exhibited a smooth microstructure, uniform pore distribution, and a gradient architecture mimicking native bone. Mechanical testing demonstrated improved compressive strength compared with individual components, and *in vitro* studies revealed stable SIM release over 24 days with a degradation profile compatible with bone regeneration. The SIM@HMSM/NP demonstrated excellent cytocompatibility, promoting the proliferation and osteogenic differentiation of bone marrow mesenchymal stem cells, and significantly enhanced bone formation in a rat calvarial defect model. These findings suggest that the SIM@HMSM/NP scaffold provides a promising strategy for sustained drug delivery and accelerated bone regeneration in critical-sized bone defects.

***Keywords*:** Bone tissue engineering; Hydrogel–scaffold composite; Hydroxyethyl methacrylate/sulfobetaine methacrylate hydrogel; Nano-hydroxyapatite/polylactic acid scaffold; Simvastatin; Three-dimensional printing

1. Introduction

Bone defects remain a major challenge in orthopedic surgery, resulting from trauma, infection, tumor resection, or congenital malformation.[1] Although minor defects can undergo spontaneous regeneration owing to the intrinsic healing capacity of bone tissue, critical-sized defects often exceed this capacity and require surgical intervention to restore function and integrity.[2] Conventional bone repair materials, such as metallic implants, polyether ether ketone, and allograft bone, have shown certain success but still suffer from inherent limitations.[3] For instance, polyether ether ketone is bioinert and lacks osteoinductivity, often resulting in poor osseointegration and fibrous tissue encapsulation.[4] Metallic implants, for instance, exhibit mismatched elastic modulus and poor biodegradability, while allografts carry risks of immune rejection and limited integration.[5] Therefore, the development of advanced bone substitutes with controllable mechanical strength, bioactivity, and biodegradability remains a pressing need to improve clinical outcomes in bone defect repair.

Hydrogels have gained increasing attention in bone tissue engineering due to their tunable physicochemical properties, high water content, and biocompatibility. Their three-dimensional (3D) network allows for nutrient diffusion, cell adhesion, and potential incorporation of bioactive molecules, making them ideal matrices for tissue regeneration.[6–8] However, traditional hydrogels are hindered by low mechanical strength and insufficient mineralization, restricting their direct application in load-bearing environments.[9] Thus, integrating mechanically robust structures with bioactive hydrogels has emerged as an effective strategy to achieve both mechanical reinforcement and osteoconductive microenvironments for bone regeneration.

Among various hydrogel systems, hydroxyethyl methacrylate (HEMA) has been extensively utilized in biomedical applications due to its favorable mechanical stability and ease of fabrication.[10] However, its application in bone repair is often limited by insufficient hydrophilicity and bioactivity, which are crucial for nutrient transport and cell adhesion. On the other hand, zwitterionic polymers, such as sulfobetaine methacrylate (SBMA), have attracted significant attention for their ability to mimic cell membrane structures, creating a super-hydrophilic hydration layer that minimizes non-specific protein adsorption and inflammation.[11] Recent studies have indicated that the copolymerization of HEMA and SBMA can synergize the mechanical robustness of HEMA with the antifouling and biocompatible properties of SBMA, resulting in a composite hydrogel named HMSM. This HMSM hybrid system thus presents a compelling candidate for bone tissue engineering, offering a tunable microenvironment that supports cellular functions while maintaining structural integrity.

However, even optimized hydrogels often fail to meet the mechanical demands of load-bearing bone defects. To address this, we integrated the bioactive HMSM hydrogel with a mechanically robust 3D-printed nano-hydroxyapatite (nHAP)/polylactic acid (PLA) (NP) scaffold. This composite strategy aims to leverage the high compressive strength of the 3D-printed framework to protect the softer, drug-loaded hydrogel matrix, thereby achieving a balance between mechanical support and biological functionality.

3D printing technology has revolutionized scaffold fabrication by enabling precise control over geometry, pore size, and internal gradient structure.[12] This technique enables scaffolds to replicate the hierarchical architecture of natural bone, which comprises cortical and trabecular regions characterized by distinct porosity and mechanical gradients. In particular, 3D-printed scaffolds composed of biodegradable polymers, such as PLA, and inorganic fillers, like nHAP, have demonstrated excellent biocompatibility and osteoconductivity.[13,14] The inclusion of nHAP enhances mineral deposition and promotes cell-mediated osteogenesis, while PLA provides mechanical integrity and biodegradability. Moreover, the NP scaffold can better match the structural and mechanical transitions of native bone, offering an optimized environment for bone tissue remodeling.[15–19]

Simvastatin (SIM), a lipophilic statin widely used for hyperlipidemia and cardiovascular diseases, has recently been identified as an osteoinductive molecule.[20,21] It can enhance bone formation by stimulating osteoblast differentiation, upregulating bone morphogenetic protein-2 (BMP-2), and promoting angiogenesis.[22–24] However, the therapeutic application of SIM in bone repair is often limited by its poor water solubility and rapid release kinetics, which may lead to transient local effects and systemic side effects upon repeated administration.[25] Therefore, developing a localized, sustained delivery system for SIM remains a critical research focus.

In this study, we developed a composite scaffold that combines a 3D-printed NP scaffold with an HMSM hydrogel for sustained SIM delivery and bone regeneration (Figure 1). The HMSM hydrogel was designed as a hydrophilic matrix to infiltrate and coat the porous scaffold, while the 3D-printed NP provided structural support and osteoconductivity. SIM was incorporated into the hydrogel–scaffold composite (denoted as SIM@HMSM/NP) to achieve localized, controlled drug release. This integrated system aims to synergistically

enhance mechanical strength, osteogenic activity, and biodegradation compatibility.

A comprehensive evaluation was conducted to assess the physicochemical characteristics, drug release profile, mechanical properties, cytocompatibility, and osteogenic efficacy of the composite both *in vitro* and *in vivo* using a critical-sized rat calvarial defect model. We hypothesized that the SIM@HMSM/NP scaffold could provide a favorable microenvironment for bone tissue regeneration, supporting sustained SIM delivery while maintaining mechanical integrity during the healing process.

2. Materials and methodology

2.1. Reagents and materials

HEMA, SBMA, and ethylene glycol dimethacrylate were purchased from Macklin Biochemical Co., Ltd. (China). SIM, ammonium persulfate (APS), N,N,N',N'-tetramethylethylenediamine (TEMED), and tannic acid (TA) were obtained from Aladdin Reagent Co., Ltd. (China). nHAP and PLA powders for 3D printing were supplied by Jinan Daigang Biomaterial Co., Ltd. (China). Alpha minimum essential medium (α-MEM) was purchased from BasalMedia Technologies, China. Fetal bovine serum was purchased from Gibco (Thermo Fisher Scientific, USA). Penicillin–streptomycin solution was obtained from Yeasen Biotechnology Co., Ltd. (China). The osteogenic induction medium contained 10 mM β-glycerophosphate, 100 nM dexamethasone, and 0.2 mM ascorbic acid (Sigma-Aldrich, USA). Calcein acetoxymethyl ester/propidium iodide (PI) live–dead cell staining kit, alkaline phosphatase (ALP) staining kit, 5-bromo-4-chloro-3-indolyl phosphate/nitro blue tetrazolium (BCIP/NBT), and Alizarin Red S (ARS) staining kit were purchased from ServiceBio (China). Hematoxylin and eosin (H&E) and Masson's trichrome staining kits were obtained from Beijing Solarbio Science & Technology Co., Ltd., China. Dylight 488- (A23210) and 594- (A23420) conjugated secondary antibodies used for immunofluorescence staining were obtained from Abbkine Scientific Co., Ltd. (China). All other reagents and solvents were of analytical grade and used without further purification. Ultrapure water (18.2 MΩ·cm) was used in all experiments.

2.2. Preparation of hydroxyethyl methacrylate/sulfobetaine methacrylate hydrogel loaded with simvastatin

A room-temperature free-radical polymerization method was employed to prepare the HMSM hydrogel loaded with SIM. Briefly, a predetermined amount of SIM was dissolved in 100 μL of deionized water under magnetic

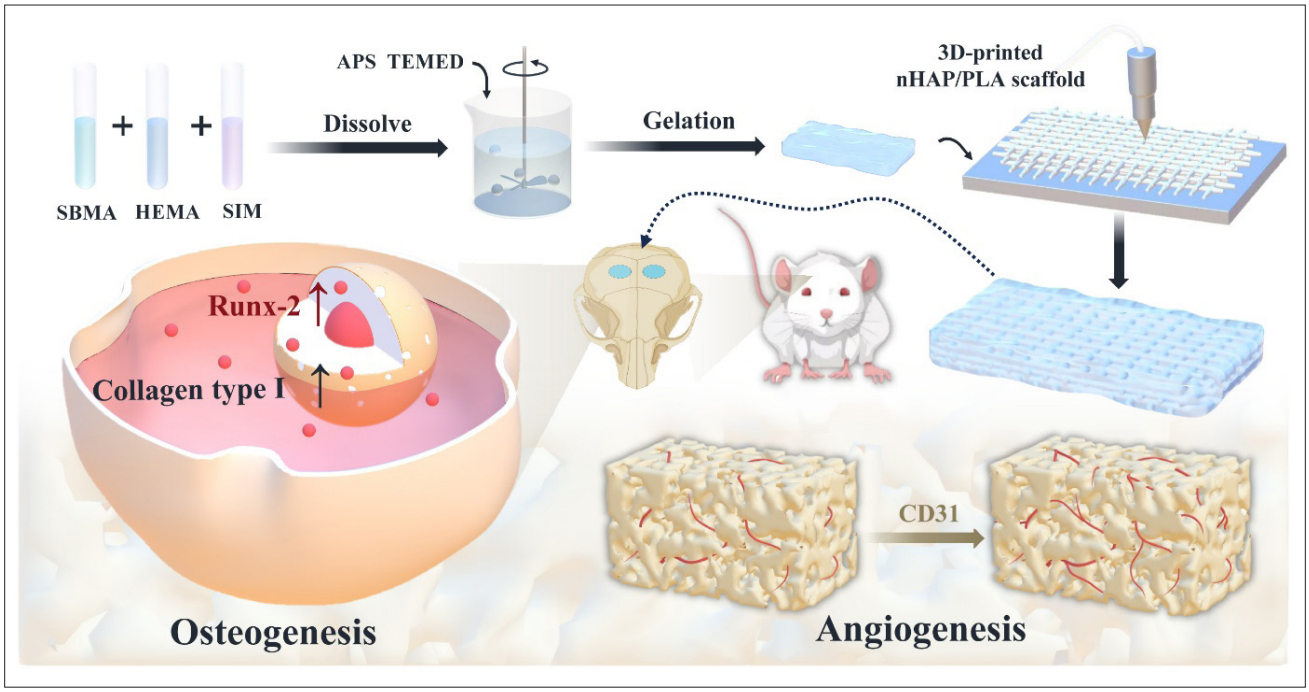

Figure 1. Schematic illustration of the SIM-loaded HEMA/SBMA hydrogel/nHAP/PLA composite scaffold for bone regeneration. The two blue dots on the rat skull indicate bilateral critical-sized calvarial defect sites. The composite scaffold promotes bone regeneration by enhancing osteogenesis, as indicated by the upregulation of Runx-2 and collagen type I, and angiogenesis, as evidenced by increased CD31 expression. Abbreviations: 3D, three-dimensional; APS, ammonium persulfate; CD, cluster of differentiation; TEMED, N,N,N',N'-tetramethylethylenediamine; SIM, simvastatin; HEMA, hydroxyethyl methacrylate; SBMA, sulfobetaine methacrylate; nHAP, nano-hydroxyapatite; PLA, polylactic acid; Runx-2, runt-related transcription factor 2.

stirring. A total of 300 μL of HEMA and 300 μL of SBMA were separately dissolved in 400 μL of Tris buffer (pH = 8.5; 10 mM) and stirred for 30 minutes at 300 rpm to obtain two solutions. Then, the two solutions were mixed and stirred for 30 minutes at 300 rpm to obtain a homogeneous solution. Subsequently, 40 μL of ethylene glycol dimethacrylate was added as a cross-linker and stirred for 15 minutes at 350 rpm. The 280 μL of SIM solution (1 mg/1 mL) was then introduced into the HEMA/SBMA mixture, followed by continuous stirring for 30 minutes at 500 rpm. Then, 5 mg of APS and 5 μL of TEMED were added as the initiator and accelerator, respectively, to initiate polymerization. Preliminary gelation occurred within 15 minutes of stirring at 150 rpm and 5 minutes of standing. All the reactions were placed at room temperature. After 24 hours of polymerization at room temperature, the hydrogel was removed, rinsed thoroughly with deionized water to eliminate unreacted monomers, and dried in an oven for further use.

2.3. *In vitro* drug release experiment of hydroxyethyl methacrylate/sulfobetaine methacrylate hydrogel loaded with simvastatin

The *in vitro* drug release behavior of the HMSM hydrogel was evaluated in phosphate-buffered saline (pH 7.4) at 37°C. Three samples of SIM-loaded hydrogels (1 g each) and three drug-free hydrogels were placed separately into 20 mL of phosphate-buffered saline solution and incubated on a constant-temperature shaker. At predetermined time intervals (0 hour, 1 hour, 3 hours, 6 hours, 9 hours, 12 hours, 18 hours, 24 hours, 3 days, 6 days, 9 days, 12 days, 18 days, and 24 days), 4 mL of the supernatant was collected and replaced with an equal volume of fresh phosphate-buffered saline. The absorbance of the withdrawn solution at 238 nm was recorded using a ultraviolet–visible spectrophotometer (Molecular Devices, USA). The cumulative release percentage of SIM was calculated based on the standard calibration curve, and the results were averaged from three independent samples.

2.4. Design and preparation of the nano-hydroxyapatite/polylactic acid scaffold

The NP scaffold was designed using computer-aided design software. Each printed scaffold had dimensions of 3 cm × 2 cm × 0.1 cm, with a line width of 300 μm and an initial pore size of 300 μm. The pore size increased by 25 μm per layer to form a gradient architecture, and each lower layer was offset by 250 μm to enhance structural stability. The scaffold was fabricated using a Low-temperature deposition manufacturing 3D printer (Bio-Architect, Regenovo, China). Before printing, PLA granules were dissolved in dichloromethane (DCM) to prepare a 15% (w/v) solution. nHAP powder was then added to the solution at a mass ratio of 1:9 (nHAP:PLA) and stirred magnetically for 24 hours to obtain a homogeneous printing ink. The printing process was conducted at room temperature with a speed of 12 mm/s and an extrusion pressure of 0.2–0.4 MPa. After printing, the scaffolds were subsequently dried at room temperature for 8 hours to allow the evaporation of DCM and at 4°C for 8 hours to remove residual solvents. Low-temperature drying was chosen because the boiling point of DCM (39.6°C) is relatively low; heating above this temperature would cause solvent boiling and potentially lead to structural defects.

2.5. Cross-linking of the drug-loaded hydrogel and the three-dimensional-printed gradient scaffold

After fabricating the 3D-printed scaffold, the SIM-loaded HMSM hydrogel precursor solution was prepared by mixing monomers, cross-linker, initiator, and SIM. TA was added to enhance interfacial adhesion. To fabricate the composite, the NP scaffold was fully immersed in the prepared SIM-loaded HMSM precursor solution (containing monomers and cross-linker) for 24 hours to ensure complete infiltration of the solution into the scaffold's micropores. Subsequently, the polymerization initiator APS and TEMED were added into the mixture to trigger *in situ* gelation. The system was allowed to react at room temperature for 24 hours, ensuring that the hydrogel formed a continuous network within and around the scaffold framework, reinforced by the addition of 2 mg of TA, for interfacial adhesion. The resulting composite (SIM@HMSM/NP) was retrieved and subjected to a rigorous purification process. Specifically, the scaffolds were immersed in a large volume of deionized water (200 mL) for 24 hours, with the water replaced every 8 hours to facilitate the diffusion and removal of unreacted monomers and residues. After washing, the scaffolds were dried in a vacuum oven for further analysis.

2.6. Scanning electron microscopy analysis

The surface morphology and microstructure of the scaffolds were characterized using scanning electron microscopy (SEM, Sigma 500, Carl Zeiss, Oberkochen, Germany). Prior to observation, the samples were freeze-dried and mounted on aluminum stubs using conductive carbon tape. All specimens were sputter-coated with a thin layer of gold to enhance electrical conductivity. SEM images were acquired at an accelerating voltage of 5–10 kV under high-vacuum conditions. Images were collected at different magnifications to evaluate the pore architecture, surface topography, and interconnectivity of the scaffolds.

2.7. Measurement of porosity

The porosity of the scaffolds was determined using the liquid displacement method based on Archimedes'

principle. Absolute ethanol was used as the displacement medium. The porosity was calculated using **Equation (1)**:

$$\text{Porosity} = (V_1 - V_3)/(V_2 - V_1) \times 100\% \quad (1)$$

where V_1 is the volume of ethanol before sample immersion, V_2 is the total volume after sample immersion, and V_3 is the remaining volume after sample removal. The calculated value represents the percentage of internal pore volume relative to the total scaffold volume.

2.8. Mechanical properties of the simvastatin@hydroxyethyl methacrylate/sulfobetaine methacrylate/nano-hydroxyapatite/polylactic acid scaffold

The mechanical properties of the HMSM hydrogel, the NP scaffold, and the composite scaffold (SIM@HMSM/NP) were tested using a universal mechanical testing machine (Zwick/Roell, Germany) under compression mode. The stress–strain curve was obtained for each sample, and the elastic modulus was calculated as the slope of the linear regression line fitted to the stress–strain data within the linear elastic region (strain range of 10–20%).

2.9. Preparation of extraction solutions of the simvastatin@hydroxyethyl methacrylate/sulfobetaine methacrylate/nano-hydroxyapatite/polylactic acid scaffold

The extraction of SIM@HMSM/NP composites was performed following a standardized protocol.[26] The HMSM hydrogel, NP scaffold, and SIM@HMSM/NP composite were cut into square specimens measuring 5 mm × 5 mm. After sterilization under ultraviolet light, each sample was immersed in complete culture medium at a surface area-to-volume ratio of 6 cm^2/mL and incubated at 37°C for 24 hours to obtain the extraction solutions. The extracts were subsequently collected, filtered through a 0.22 μm membrane to remove particulates, and stored at 4°C for subsequent biocompatibility and osteogenic evaluations.

2.10. Biocompatibility evaluation and live/dead staining

To evaluate cytocompatibility, the hydrogel and composite samples were pre-soaked in complete culture medium overnight to remove residual monomers. Bone marrow mesenchymal stem cells (BMSCs, 1×10^5 cells per well) were then seeded onto the surface of the SIM@HMSM/NP composites in 24-well plates and incubated under standard culture conditions. After 7 days of co-culture, cell viability was assessed using a calcein acetoxymethyl ester/PI staining kit, following the manufacturer's instructions. A Transwell indirect co-culture assay was further employed to assess potential cytotoxicity.[27] Briefly, hydrogel samples were placed in the upper chamber of a Transwell insert (pore size 3 μm; Cat. No. TCS019024, Jet Biofil, China), while BMSCs were seeded in the lower chamber. After 3 days of co-culture, live/dead staining was performed as described above. The stained cells were imaged using an inverted fluorescence microscope (ECLIPSE Ts2R, Nikon, Japan) or a confocal laser scanning microscope (STELLARIS 5, Carl Zeiss, Germany). To quantitatively assess cell proliferation, a Cell Counting Kit-8 (CCK-8) assay was performed. BMSCs were seeded on the scaffolds in 24-well plates at a density of 1×10^4 cells per well. At predetermined time points (1, 3, and 5 days), the culture medium was replaced with fresh medium containing 10% CCK-8 solution. After incubation for 2 hours at 37°C, the absorbance of the supernatant was measured at 450 nm using a microplate reader (Molecular Devices, USA). All experiments were performed in triplicate.

2.11. *In vitro* evaluation of osteogenic properties of the simvastatin@hydroxyethyl methacrylate/sulfobetaine methacrylate/nano-hydroxyapatite/polylactic acid scaffold

To evaluate the osteogenic potential of the composites, extraction solutions from different material groups were co-cultured with BMSCs. After 7 days of incubation, alkaline phosphatase staining was performed using a BCIP/NBT chromogenic substrate kit (ServiceBio, China) to visualize ALP activity and assess early-stage osteogenic differentiation. Mineralization was further evaluated on day 21 by ARS staining to detect calcium nodule formation under a light microscope. In addition, immunofluorescence staining was conducted to analyze the expression of osteogenesis-related proteins, including collagen type I (Col-I) and runt-related transcription factor 2 (Runx-2). Dylight 488- or 594-conjugated secondary antibodies (1:200) were used for fluorescent labeling, and images were captured using a fluorescence microscope (ECLIPSE Ts2R, Nikon, Japan).

2.12. Cell lines and animals

All animal procedures were reviewed and approved by the Laboratory Animal Management and Ethics Committee of Qingdao University (Approval No. 20220910) and conducted in accordance with the Guidelines for the Care and Use of Laboratory Animals (National Research Council, USA) and the Guidelines for the Ethical Review of Experimental Animals in the People's Republic of China (GB/T 35892-2018). Healthy male Sprague–Dawley (SD) rats (n = 48), aged approximately 8 weeks and weighing 250–300 g, were obtained from the Fushan Campus of Qingdao University. The animals were housed under standard laboratory conditions (temperature 22 ± 2°C,

relative humidity 55 ± 5%, 12 hours light/dark cycle) with free access to food and water. The rats were randomly divided into four groups (n = 12 per group): (i) blank group (Blank): defect left unfilled without any material implantation; (ii) hydrogel group (HMSM): implantation of HMSM hydrogel; (iii) scaffold group (NP): implantation of 3D-printed NP scaffold; and (iv) composite group (SIM@HMSM/NP): implantation of SIM-loaded hydrogel–scaffold composite. BMSCs were isolated from 4-week-old male SD rats following standard procedures. BMSCs were maintained in α-MEM supplemented with 10% fetal bovine serum and 1% penicillin–streptomycin under standard culture conditions (37°C, 5% carbon dioxide, humidified atmosphere). The culture medium was refreshed every 2 days. For osteogenic induction, BMSCs were cultured in α-MEM containing 10 mM β-glycerophosphate, 100 nM dexamethasone, and 0.2 mM ascorbic acid for the indicated time periods prior to further analysis.

2.13. *In vivo* bone formation assessment

A critical-sized cranial defect model was established in 8-week-old male SD rats (250–300 g) to evaluate *in vivo* bone formation as previously reported.[28] A full-thickness circular defect (5 mm in diameter) was created on the parietal bone using an electric trephine drill under continuous saline irrigation to avoid thermal injury. The defect sites were treated according to the experimental grouping: Blank, HMSM, NP, and SIM@HMSM/NP. After implantation, the periosteum and skin were sutured in layers. At 4 and 8 weeks postoperatively, the rats were euthanized, and the calvarial specimens were harvested and fixed in 10% paraformaldehyde. Micro-computed tomography (Micro-CT; Bruker, USA) was performed to assess new bone formation, and the data were analyzed using CTAn software (version 1.18.4.0) to quantify bone volume fraction (BV/TV). The fixed samples were then decalcified, dehydrated, and embedded in paraffin. Sections (5 μm thick) were prepared for histological analysis, including H&E and Masson's trichrome staining, to evaluate bone matrix deposition and collagen organization. Additionally, immunofluorescence staining was performed to detect osteogenic and angiogenic markers, including Col-I and cluster of differentiation 31 (CD31), using Dylight 488- and 594-conjugated secondary antibodies (1:200), respectively. Images were captured using a fluorescence microscope (ECLIPSE Ts2R, Nikon, Japan).

2.14. Statistical analysis

All data were expressed as mean ± standard deviation (mean ± SD). Differences among groups were evaluated by one-way analysis of variance followed by Tukey's post hoc multiple comparison test. A p-value of less than 0.05 was considered statistically significant. Statistical significance levels were denoted as $p < 0.05$. GraphPad Prism software (version 9.0, GraphPad software, USA) was used for data visualization and figure preparation.

3. Results and discussion

3.1. Preparation of hydroxyethyl methacrylate/sulfobetaine methacrylate hydrogel loaded with simvastatin

The development of an effective drug delivery matrix with mechanical robustness is essential for bone tissue engineering. Hydrogels have been widely explored as localized drug carriers owing to their high biocompatibility, adjustable cross-linking density, and ability to sustain therapeutic release.[29] However, single-component hydrogels such as HEMA or SBMA often face limitations: HEMA hydrogels provide good mechanical strength but poor water absorption, whereas SBMA hydrogels exhibit outstanding hydrophilicity yet insufficient mechanical integrity.[30,31]

By co-polymerizing HEMA and SBMA, the HMSM hydrogel combines the complementary advantages of both monomers, resulting in improved flexibility, enhanced water retention, and improved surface compatibility. The incorporation of SIM into the HMSM network enables localized drug loading, while integration with a 3D-printed NP scaffold further enhances mechanical stability and osteoconductivity. The SIM@HMSM/NP was constructed by integrating chemical polymerization and 3D-printing technologies. The free radical polymerization of HEMA and SBMA, initiated by APS/TEMED, led to the formation of a cross-linked HMSM hydrogel network capable of encapsulating SIM. The zwitterionic SBMA component imparted strong hydration and antifouling properties through electrostatic charge balance, while HEMA provided structural stability to the hydrogel matrix.

The pre-formed HMSM precursor was introduced into the 3D-printed NP scaffold, where *in situ* gelation occurred, filling the scaffold pores and ensuring intimate interfacial adhesion between the polymeric and inorganic phases. This hybrid design combines the high biocompatibility and sustained release capacity of the hydrogel with the mechanical strength and osteoconductivity of the NP framework.

In Figure 2A–I, the hydrogel exhibited a transparent, uniform texture, while the 3D-printed scaffold presented a well-defined gradient porous structure. SEM analysis confirmed smooth surfaces for HMSM, regular and interconnected pores for NP, and cohesive integration in the SIM@HMSM/NP without interfacial delamination. As shown in Figure 2C–D, the NP scaffold was designed using computer-aided design software and fabricated through

3D printing with precise control of pore geometry and filament arrangement. The scaffold exhibited a rectangular shape (3 cm × 2 cm × 0.1 cm) with a uniform, grid-like pattern. The surface layer was composed of printed filaments with a diameter of approximately 300 μm and a pore size of 300 μm, while the pore size gradually increased to 500 μm in the lower layers, with a 25 μm increment per layer. This gradient structural design was specifically engineered to validate the concept of bionic repair. By mimicking the transition from dense cortical bone to porous trabecular bone, the scaffold achieves a functional balance: the upper layers with smaller pores provide necessary mechanical shielding and structural integrity, while the lower layers with larger pores create an open microenvironment. This open structure is critical for minimizing resistance to nutrient diffusion and facilitating the deep ingrowth of blood vessels and bone tissue, as distinct from uniform scaffolds, which often suffer from necrotic cores due to poor perfusion. The success of this design is evidenced by the superior mechanical properties (Figure 3C) and the uniform bone formation observed in the critical-sized defect model. This programmed gradient created a hierarchical internal architecture with distinct layer-by-layer offsets, providing larger interspaces toward the base of the scaffold. Such a gradient configuration not only enhances the mechanical stability of the construct but also increases its capacity to retain and distribute hydrogel or drug molecules evenly within the pores.[2,32,33] The enlarged internal channels facilitate deeper penetration of the HMSM hydrogel during *in situ* gelation, which is expected to reduce the initial burst release and promote a more sustained and uniform drug delivery profile during subsequent degradation. These structural features collectively contribute to improved mechanical reinforcement and bioactivity, laying a robust foundation for effective bone tissue regeneration.

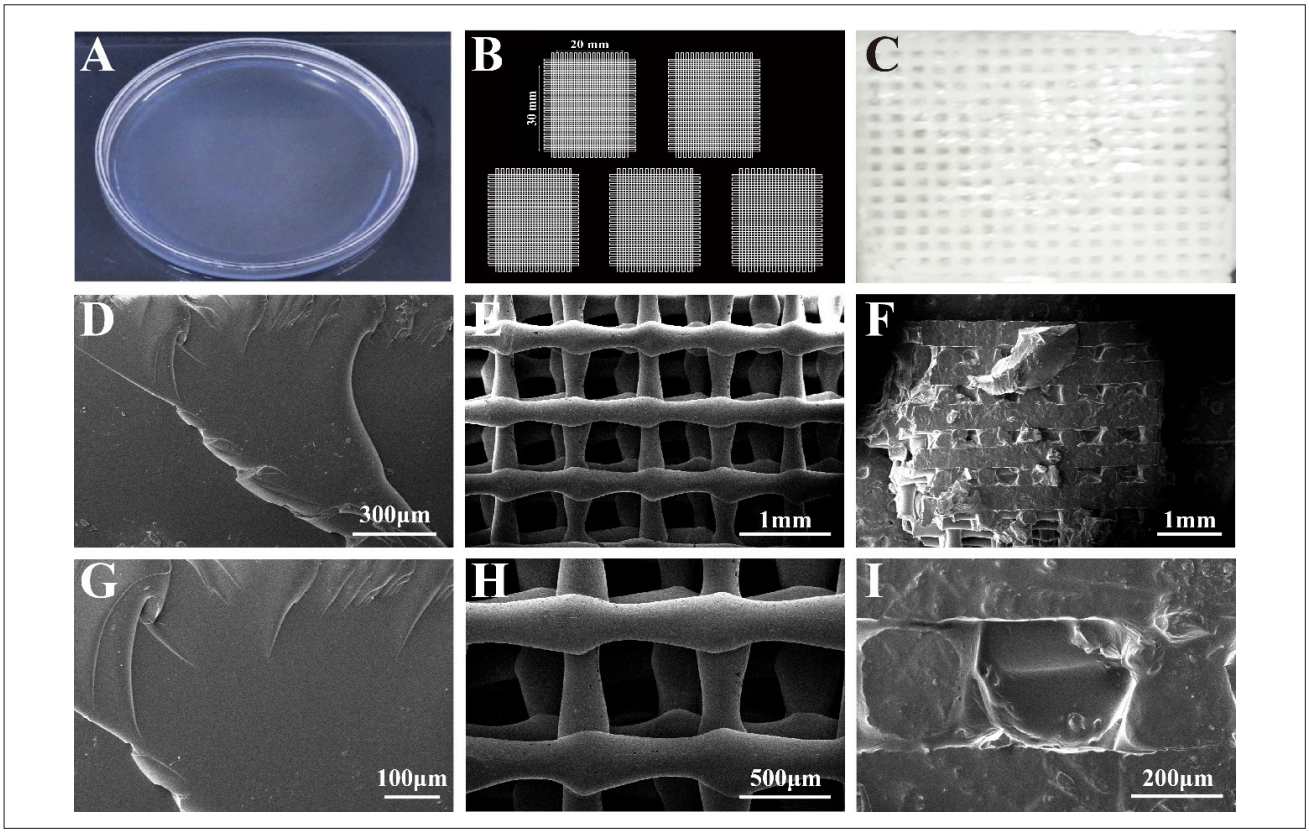

Figure 2. Fabrication process and morphological characterization of the SIM@HMSM/NP composite scaffold. (A) Photograph of the synthesized HMSM hydrogel exhibiting a transparent and homogeneous appearance. (B) Computer-aided design of the 3D-printed NP scaffold with precise pore control. (C) Optical image of the printed scaffold showing a uniform, interconnected framework. (D & G) SEM images of the HMSM hydrogel showing a smooth surface and dense polymeric morphology. Scale bars: 100 μm, 300 μm; magnifications: 200× & 1000×. (E & H) SEM images of the 3D-printed NP scaffold demonstrating well-ordered gradient pores and regular filament arrangement. Scale bars: 1 mm, 500 μm; magnifications: 1000× & 2000×. (F & I) SEM images of the SIM@HMSM/NP revealing tight interfacial bonding between the hydrogel and scaffold with continuous, integrated pore structures. Scale bars: 1 mm, 200 μm; magnifications: 200× & 2000×. Abbreviations: 3D, three-dimensional; HMSM, hydroxyethyl methacrylate/sulfobetaine methacrylate; NP, nano-hydroxyapatite/polylactic acid; SEM, scanning electron microscopy; SIM, simvastatin.

3.2. Characterizations of simvastatin @hydroxyethyl methacrylate/sulfobetaine methacrylate/nano-hydroxyapatite/polylactic acid hydrogel

The NP scaffold was fabricated with precisely controlled pore architecture and uniform layer alignment (Figure 3A–D). Mechanical testing revealed that the HMSM hydrogel exhibited an elastic modulus of 2.18 ± 0.287 MPa, while the NP scaffold reached 16.95 ± 2.36 MPa. Notably, the SIM@HMSM/NP composite showed the highest modulus of 24.17 ± 4.27 MPa, surpassing both human cancellous bone (3.2–12.8 MPa) and cortical bone (17–20 MPa), indicating sufficient mechanical strength for bone defect support. Based on the liquid displacement method, the porosity of the NP scaffold was calculated to be 46.22 ± 1.01%. This value falls well within the optimal range (40–70%) required for bone tissue engineering applications. Such a porous structure is conducive to nutrient transport and provides sufficient space for cell adhesion and proliferation, which is essential for facilitating subsequent neovascularization and bone ingrowth. Furthermore, the water absorption capability is a vital parameter for hydrogel-based composites, as it influences nutrient diffusion and metabolic waste removal. As shown in Figure 3E, the HMSM hydrogel exhibited a high swelling ratio due to its hydrophilic nature. The SIM@HMSM/NP composite also demonstrated significant water absorption. This swelling behavior ensures that the composite can effectively absorb tissue fluids upon implantation, creating a moist microenvironment conducive to cell survival and recruitment. In the degradation assay, the SIM@HMSM/NP composite exhibited a gradual mass loss of 42.82 ± 3.18% after 28 days (Figure 3D). Interestingly, this degradation rate was slightly higher than that of the pure HMSM hydrogel. This phenomenon can be attributed to the "restricted swelling" effect: the rigid NP scaffold constrains the volume expansion of the hydrophilic HMSM hydrogel. The resulting internal swelling stress may induce micro-cracking and accelerated fragmentation of the hydrogel network within the pores. Additionally, the porous architecture of the scaffold increases the specific surface area of the hydrogel exposed to the medium, further facilitating hydrolytic degradation. This degradation profile corresponds well with the pace of natural bone regeneration.[34] This controlled degradation ensures that the scaffold maintains temporary mechanical integrity while gradually providing space for new bone ingrowth.

The quantification of SIM concentration was determined using a standard calibration curve, which showed a good linear relationship (Figure 3A). Drug release analysis (Figure 3B) showed an initial mild release followed by a sustained phase over 24 days, suggesting that the hydrogel–scaffold composite effectively reduces early burst release and maintains long-term drug availability. It is important to note that the drug release behavior is intrinsically governed by the structural parameters of the composite system. In this study, the formulation was optimized to balance mechanical strength and biological activity. The release mechanism is twofold. First, the dense cross-linked network of the HMSM hydrogel acts as the primary diffusion barrier, regulating the migration of SIM molecules. Second, the 3D-printed NP scaffold imposes a geometric constraint. Unlike a free-swelling hydrogel, the hydrogel within the composite is confined within the scaffold struts, which limits the effective surface area exposed to the surrounding fluid. This structural confinement prevents rapid bulk degradation and burst release, thereby extending the therapeutic window. While varying the pore size or hydrogel cross-linking density could further tune the release kinetics, the current parameters were chosen to prioritize mechanical stability and a conducive pore size for osteoblast infiltration. Collectively, these findings confirm that the SIM@HMSM/NP composite achieves a desirable balance between mechanical stability, biodegradability, and sustained drug delivery, which are essential parameters for bone tissue regeneration.

3.3. Biocompatibility of composite materials

Good biocompatibility is a prerequisite for the application of hydrogels in tissue engineering, as it directly influences cellular behavior and regenerative outcomes.[35] To comprehensively assess the cytocompatibility of the HMSM hydrogel, NP scaffold, and SIM@HMSM/NP composite, both direct and indirect co-culture assays were performed (Figure 4A–C). In the direct co-culture setup, fluorescently labeled BMSCs were observed to be distributed as discrete punctate signals on the surface of SIM@HMSM/NP, indicating successful cell attachment and survival. Although the intrinsic fluorescence of the scaffold resulted in a green background signal, the presence of distinct cell-associated fluorescence confirmed the cytocompatibility of the composite scaffold (Figure 4B). In the Transwell indirect co-culture system, live/dead staining showed predominant green fluorescence across all groups, confirming high cell viability and minimal cytotoxicity (Figure 4C). This observation was further supported by quantitative analysis of the percentage of live cells (Figure 4E), which showed no significant differences among the control, HMSM, NP, and SIM@HMSM/NP groups.

Compared with the control, both HMSM hydrogel and NP scaffold maintained favorable cell survival, while the SIM@HMSM/NP composite exhibited excellent biocompatibility, supporting robust BMSC proliferation and uniform distribution similar to the control groups. These results indicate that the incorporation of SIM and

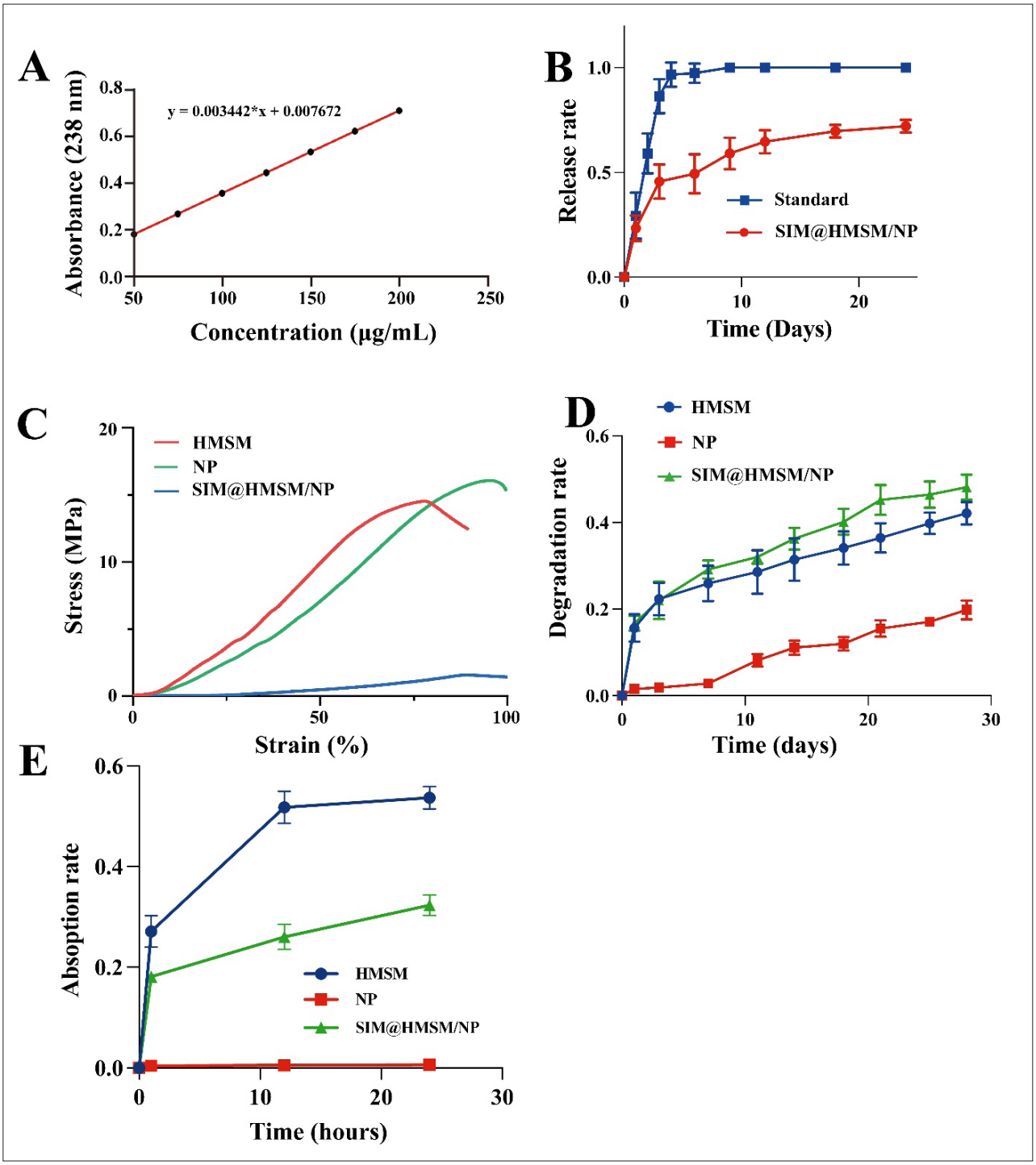

Figure 3. Physicochemical and mechanical characterization of HMSM hydrogel, NP scaffold, and SIM@HMSM/NP composite scaffold. (A) Standard calibration curve of SIM at 238 nm showing linear correlation between absorbance and concentration ($y = 0.003442 \times x + 0.007672$, $R^2 = 0.998$), confirming reliable quantification for release analysis. (B) Cumulative drug release profiles of SIM@HMSM/NP composite and free SIM standard solution over 24 days, indicating a sustained and controlled release behavior in the composite scaffold. (C) Compressive stress–strain curves of HMSM hydrogel, NP scaffold, and SIM@HMSM/NP composite. The composite exhibited the highest elastic modulus (24.17 ± 4.27 MPa), surpassing both individual components and aligning with the mechanical range of natural bone. (D) *In vitro* degradation profiles of HMSM hydrogel, NP scaffold, and SIM@HMSM/NP composite over 28 days. The composite displayed gradual mass loss (42.82 ± 3.18%), suggesting balanced biodegradability compatible with bone tissue regeneration. (E) Water absorption behavior of the scaffolds. The experiments were performed in triplicate. Data are presented as mean ± standard deviation ($n = 3$). Abbreviations: HMSM, hydroxyethyl methacrylate/sulfobetaine methacrylate; NP, nano-hydroxyapatite/polylactic acid; SIM, simvastatin.

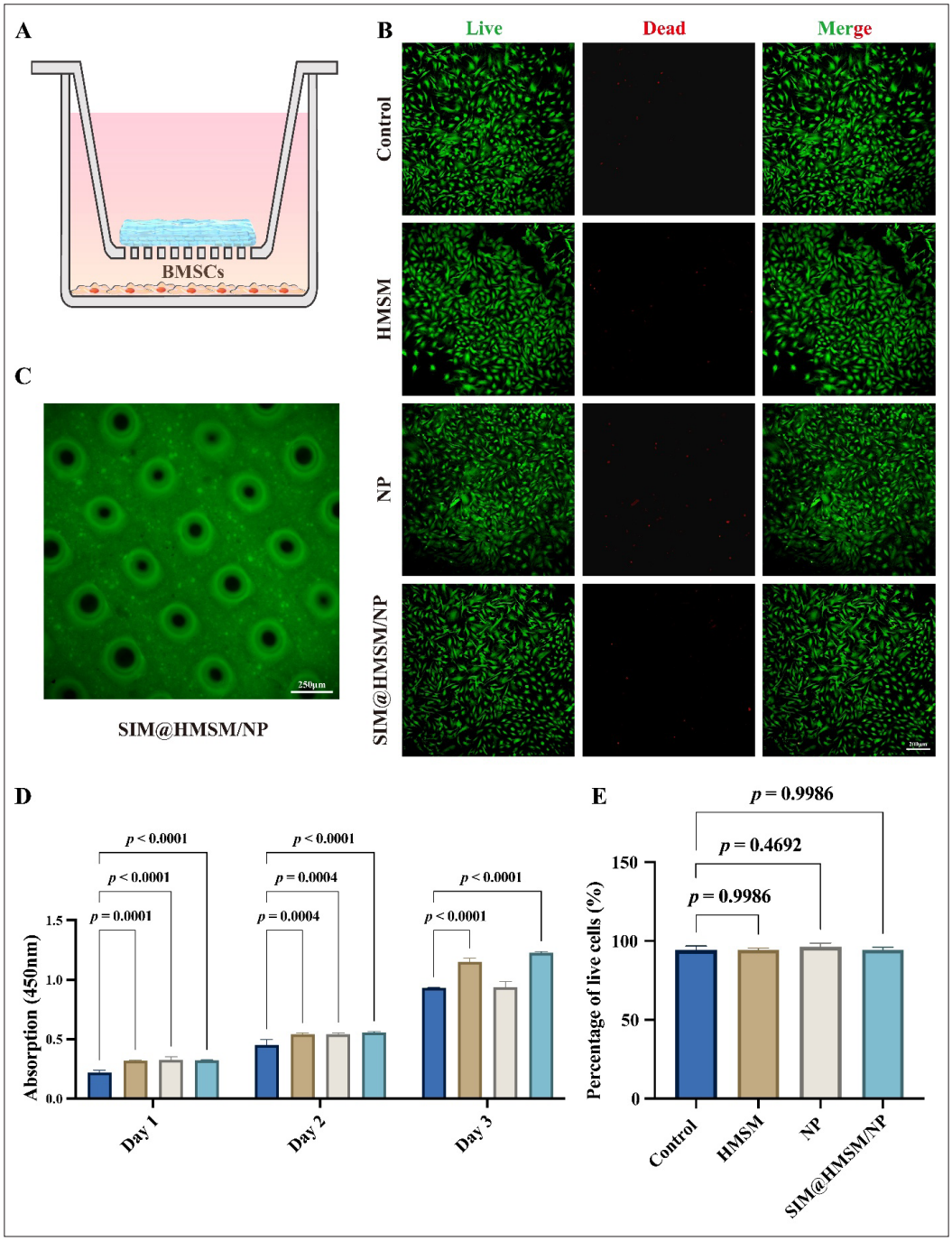

Figure 4. Cytocompatibility evaluation of HMSM hydrogel, NP scaffold, and SIM@HMSM/NP composite using calcein AM/PI staining. (A) Schematic illustration of the Transwell co-culture setup used for cytocompatibility testing. SIM@HMSM/NP composites were placed in the upper chamber, while BMSCs were cultured in the lower chamber to assess indirect cytotoxicity. (B) Live/dead staining of BMSCs directly co-cultured with the SIM@HMSM/NP composite, showing extensive cell survival and uniform cell attachment on the material surface. Scale bar: 250 μm; magnification: 10×. (C) Representative fluorescence images of BMSCs after 3 days of indirect co-culture with different material extracts (control, HMSM, NP, and SIM@HMSM/NP). Green fluorescence (calcein AM) indicates live cells, and red fluorescence (PI) indicates dead cells. Scale bar: 200 μm; magnification: 20×. (D) Quantitative analysis of BMSC proliferation evaluated by the CCK-8 assay at days 1, 2, and 3. The absorbance at 450 nm increased over time in all groups, demonstrating continuous cell proliferation and confirming that none of the materials inhibited cell growth. (E) Quantitative analysis of cell viability expressed as the percentage of live cells, showing no significant differences among the control, HMSM, NP, and SIM@HMSM/NP groups, further confirming excellent cytocompatibility. Data are presented as mean ± standard deviation (n = 3). Abbreviations: AM, acetoxymethyl ester; HMSM, hydroxyethyl methacrylate/sulfobetaine methacrylate; NP, nano-hydroxyapatite/polylactic acid; PI, propidium iodide; SIM, simvastatin; BMSCs, bone marrow-derived mesenchymal stem cells.

the hybridization of hydrogel with the 3D-printed scaffold did not compromise biocompatibility but provided a more conducive microenvironment for cell growth. Quantitative analysis via the CCK-8 assay (Figure 3D) further corroborated these findings. The optical density (OD) values in all groups increased continuously from day 1 to day 5, indicating active cell proliferation. The SIM@HMSM/NP group showed slightly higher OD values than the control group, demonstrating that the composite scaffold supports BMSC viability and proliferation.

3.4. *In vitro* osteogenic performance of composite materials

To assess the osteogenic potential of the composite materials, BMSCs were cultured in extraction solutions from different groups and subjected to ALP, ARS, and immunofluorescence analyses (Figure 5A–D). After 7 days, ALP staining revealed pronounced blue coloration in the SIM@HMSM/NP group, suggesting enhanced early osteogenic differentiation compared with HMSM and NP alone. By day 21, ARS staining showed dense red calcium nodules, indicating active mineralization and late-stage osteogenesis. Quantitative analysis confirmed that ALP activity in the SIM@HMSM/NP group was significantly higher than in the HMSM, NP, or control groups ($p < 0.0001$) (Figure 5B). Immunofluorescence results further validated these findings. As shown in Figure 5C, both Runx-2 and Col-I exhibited markedly increased fluorescence intensity in the SIM@HMSM/NP group. Statistical analysis (Figure 5D) demonstrated that Runx-2 expression increased approximately 2.8-fold and Col-I expression 3.1-fold compared with the control group ($p < 0.0001$). These results indicate that the composite scaffold not only supports cell survival but also effectively promotes osteogenic differentiation.

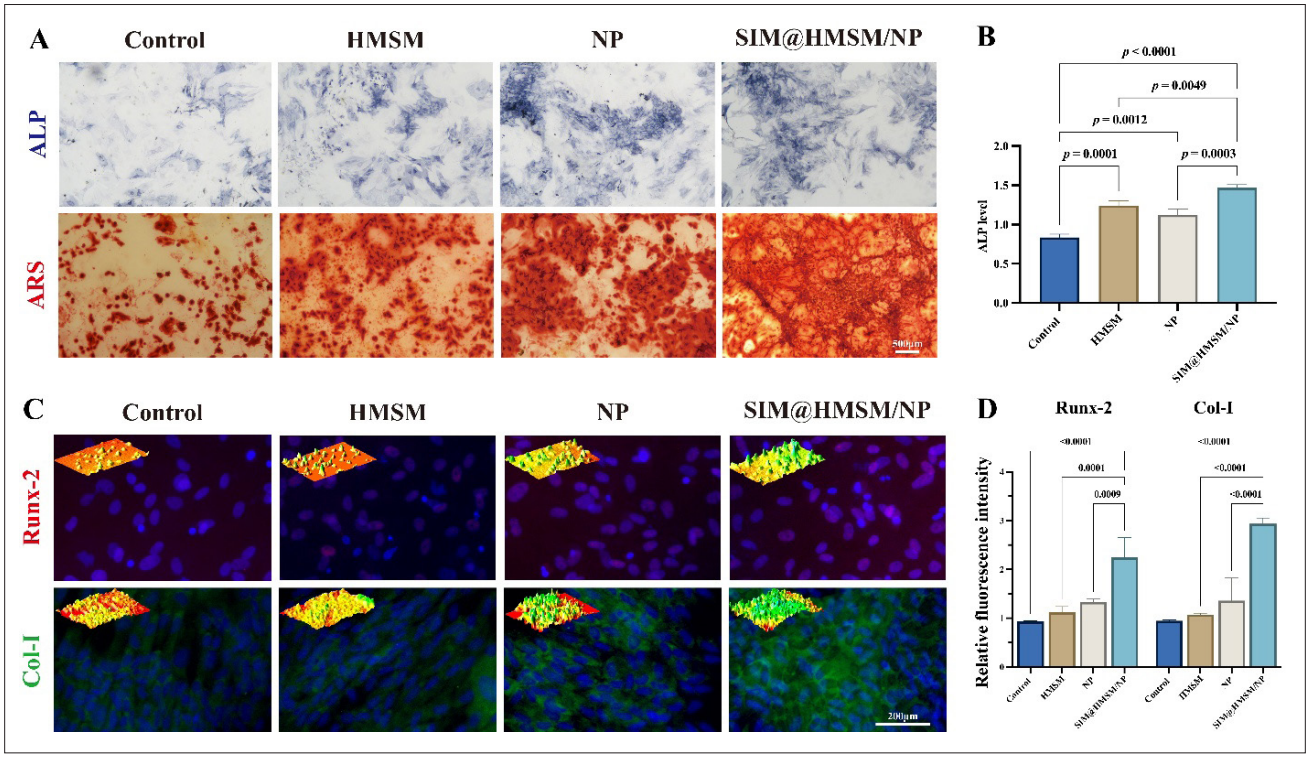

Figure 5. Osteogenic differentiation of BMSCs cultured with extracts from different materials. (A) Representative images of ALP staining at day 7 (upper panels) and ARS staining at day 21 (lower panels) in different extract groups (control, HMSM, NP, and SIM@HMSM/NP). In the ALP images, purple/blue coloration indicates ALP-positive regions, reflecting early osteogenic differentiation, while in the ARS images, red-stained areas represent calcium-rich mineralized nodules, indicating late-stage mineralization. Scale bar: 500 μm; magnification: 10×. (B) Quantitative analysis of ALP activity, showing significantly higher ALP levels in the SIM@HMSM/NP group compared with the other groups ($p < 0.0001$). (C) Immunofluorescence staining of osteogenic markers Runx-2 and Col-I in BMSCs after 14 days of culture. Protein expression is visualized using pseudo-colored fluorescence intensity maps, while cell nuclei were counterstained with DAPI (blue). Scale bar: 200 μm; magnification: 20×. (D) Quantification of fluorescence intensity demonstrating significantly increased Runx-2 and Col-I expression in the SIM@HMSM/NP group compared with the other treatments ($p < 0.0001$). Data are presented as mean ± standard deviation ($n = 3$). Abbreviations: ALP, alkaline phosphatase; ARS, Alizarin Red S; BMSCs, bone marrow-derived stem cells; Col-I, collagen type 1; DAPI, 4',6-diamidino-2-phenylindole; HMSM, hydroxyethyl methacrylate/sulfobetaine methacrylate; NP, nano-hydroxyapatite/polylactic acid; Runx-2, runt-related transcription factor 2; SIM, simvastatin.

This enhancement can be attributed to the synergistic effects of SIM and the bioactive NP framework. SIM is known to upregulate BMP-2 and activate Runx-2 signaling pathways, while nHAP provides osteoconductive cues that promote calcium phosphate deposition.[36] The incorporation of HMSM hydrogel further ensures localized, sustained release of SIM, maintaining effective concentrations at the cell–material interface. Together, these factors establish a favorable osteoinductive microenvironment conducive to bone tissue regeneration.

3.5. *In vivo* osteogenic performance of composite materials

To further assess the osteogenic performance of the composite materials *in vivo*, a critical-sized rat calvarial defect model was used to evaluate bone regeneration at 4 and 8 weeks post-implantation (Figure 6A–C). Micro-CT 3D reconstruction demonstrated that the control group retained large unhealed regions, while defects treated with HMSM or NP scaffolds exhibited limited bone ingrowth. In contrast, the SIM@HMSM/NP group showed continuous new bone formation and

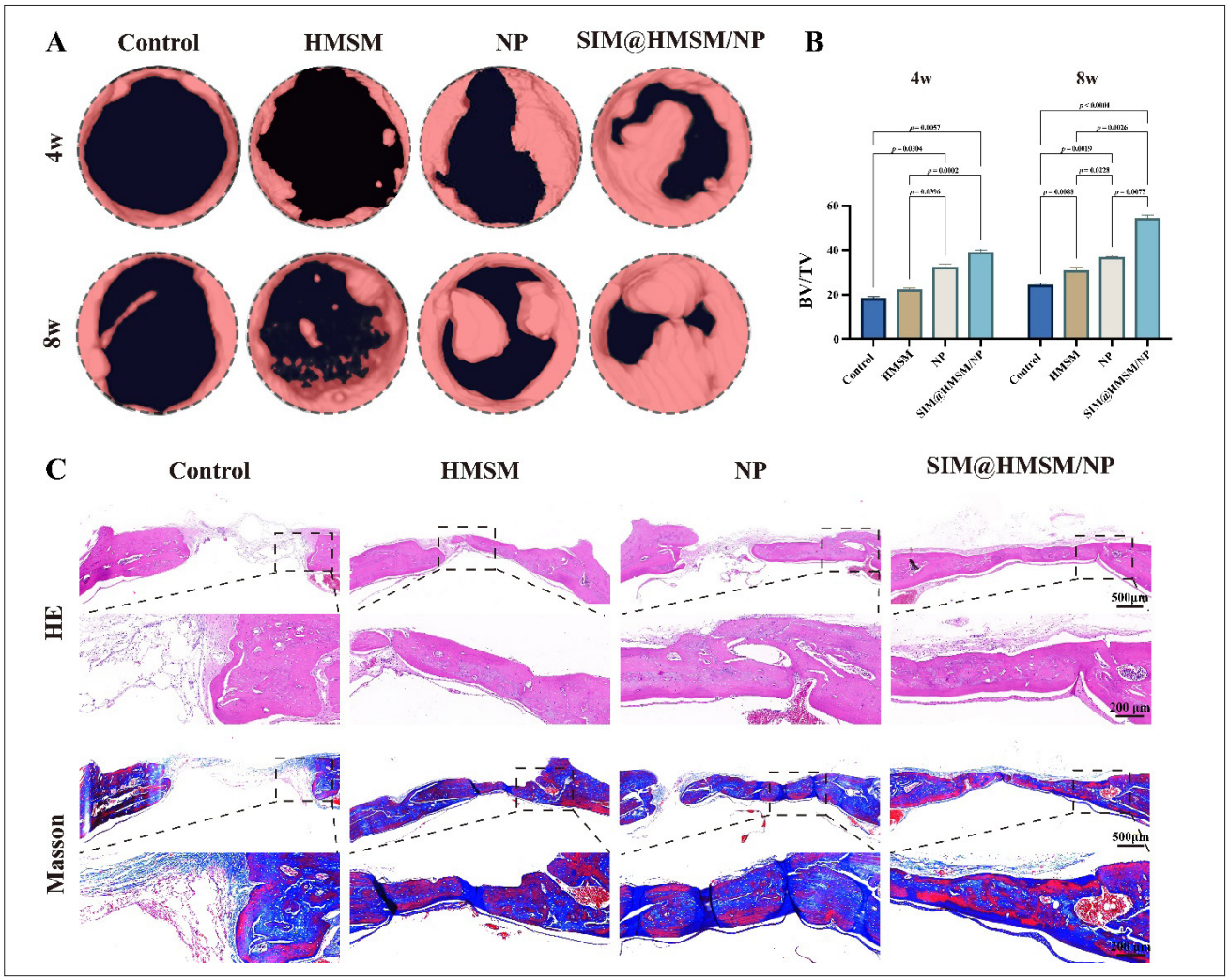

Figure 6 *In vivo* bone regeneration in rat calvarial defects treated with different materials. (A) Three-dimensional micro-CT reconstruction images of cranial bone defects at 4 and 8 weeks post-implantation in different treatment groups (control, HMSM, NP, and SIM@HMSM/NP). The SIM@HMSM/NP group exhibited markedly enhanced bone formation and defect bridging compared with other groups. (B) Quantitative analysis of BV/TV derived from micro-CT data, showing significantly higher bone regeneration in the SIM@HMSM/NP group than in the HMSM, NP, and control groups ($p < 0.001$). (C) Representative histological sections stained with H&E and Masson's trichrome at 8 weeks. H&E staining revealed abundant new bone trabeculae and well-integrated bone tissue in the SIM@HMSM/NP group, while Masson's staining confirmed dense collagen deposition and mature bone matrix formation. Scale bars: 200 and 500 μm; magnifications: 20× & 2×. Data are presented as mean ± standard deviation. For each group at each time point, $n = 6$ independent biological replicates were analyzed. Abbreviations: CT, computed tomography; HMSM, hydroxyethyl methacrylate/sulfobetaine methacrylate; NP, nano-hydroxyapatite/polylactic acid; SIM, simvastatin; BV/TV, bone volume fraction; H&E, hematoxylin and eosin; SIM, simvastatin.

near-complete bridging of the defect area by week 8. Quantitative micro-CT analysis revealed that the BV/TV in the SIM@HMSM/NP group was significantly higher than in the other groups at both 4 and 8 weeks ($p < 0.001$) (Figure 6B). These findings indicate that the incorporation of SIM markedly enhanced osteogenesis within the composite scaffold, consistent with its known ability to stimulate BMP-2 expression and activate the Runx-2 pathway. Histological staining further corroborated the imaging results. H&E staining revealed extensive formation of new trabecular bone with a well-organized structure in the SIM@HMSM/NP group, while the control and single-material groups showed only partial repair (Figure 6C). Masson's trichrome staining exhibited dense blue-stained collagen fibers and well-mineralized bone tissue in the SIM@HMSM/NP group, confirming active matrix deposition and tissue maturation.

Collectively, these results demonstrate that the SIM@HMSM/NP not only accelerates bone defect healing but also promotes the formation of mature, vascularized bone tissue, validating its potential for clinical application in bone regeneration. It is worth noting that while the current study demonstrated significant bone regeneration and near-complete defect bridging within 8 weeks, the complete remodeling of the calvarial defect may require a longer observation period. Future studies should extend the *in vivo* evaluation to 12 or 16 weeks to further investigate the long-term degradation behavior of the scaffold and the complete maturation process of the regenerated bone tissue.

3.6. Angiogenic and osteogenic coupling within regenerated bone tissue

Recent advances highlight that effective bone regeneration relies not only on osteogenic differentiation but also on coordinated vascularization, a process defined as angiogenic–osteogenic coupling.[37,38] For example, SIM-loaded scaffolds have been shown to simultaneously enhance new bone formation and neovascularization *in vivo*.[39] Scaffold designs that integrate angiogenic cues and osteogenic cues are thus emerging as a key strategy in bone tissue engineering.[40] To elucidate the interplay between angiogenesis and osteogenesis during bone repair, immunofluorescence staining for CD31 and Col-I was conducted on calvarial sections harvested at 8 weeks (Figure 7). In the control and single-material groups (HMSM and NP), only sparse CD31-positive vessels were observed within the defect area, suggesting limited

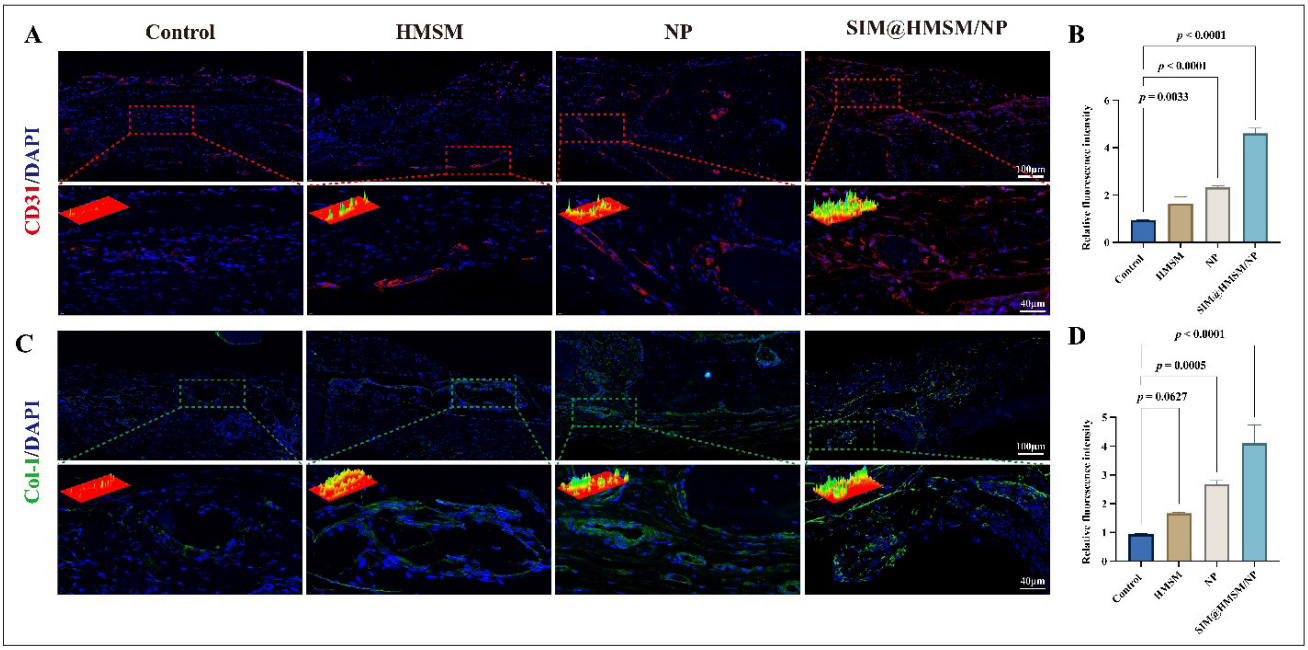

Figure 7. Immunofluorescence analysis of angiogenesis and bone matrix formation in regenerated calvarial tissue. (A) Representative immunofluorescence images of cranial defect sections stained for the vascular endothelial marker CD31 (red), with cell nuclei counterstained by DAPI (blue), showing neovascular distribution in different groups (control, HMSM, NP, and SIM@HMSM/NP). Scale bars: 40 & 100 μm; magnifications: 100× & 40×. (B) Quantitative analysis of relative CD31 fluorescence intensity. (C) Immunofluorescence staining of Col-I (green) with DAPI (blue), illustrating collagen deposition and bone matrix formation in the regenerated tissue. Scale bars: 40 & 100 μm; magnifications: 100× & 40×. (D) Quantitative analysis of relative Col-I fluorescence intensity. Data are presented as mean ± SD ($n = 6$), and statistical significance was determined by one-way analysis of variance. Abbreviations: CD, cluster of differentiation; Col-I, collagen type 1; DAPI, 4',6-diamidino-2-phenylindole; HMSM, hydroxyethyl methacrylate/sulfobetaine methacrylate; NP, nano-hydroxyapatite/polylactic acid; SIM, simvastatin.

neovascularization. In contrast, the SIM@HMSM/NP group exhibited extensive CD31 expression surrounding newly formed bone trabeculae, indicating the formation of a dense microvascular network that supports active tissue regeneration. Similarly, Col-I staining revealed markedly enhanced collagen deposition in the SIM@HMSM/NP group compared with the other groups, reflecting vigorous extracellular matrix production and maturation of regenerated bone tissue. The 3D fluorescence intensity analysis confirmed that both CD31 and Col-I signals were significantly upregulated in the SIM@HMSM/NP group, consistent with the micro-CT and histological results (Figures 6A–C).

These findings demonstrate that the SIM@HMSM/NP effectively promotes osteogenic–angiogenic coupling—a critical process for successful bone regeneration. The sustained release of SIM likely plays a dual regulatory role by upregulating vascular endothelial growth factor and BMP-2 pathways, thereby stimulating endothelial cell proliferation and osteoblast differentiation simultaneously. This coordinated effect enhances nutrient supply, matrix deposition, and tissue integration, collectively accelerating defect healing and functional bone restoration.

The SIM@HMSM/NP group exhibited significantly higher CD31 and Col-I expression compared with the other groups, indicating enhanced angiogenesis and bone matrix formation.

4. Conclusion

In recent years, increasing attention has been paid to advanced hydrogel systems for bone regeneration, including injectable and self-healing hydrogels, supramolecular hydrogels, and shape–memory hydrogels fabricated by 3D printing. These systems enable minimally invasive delivery, dynamic structural adaptation, and programmable drug release behavior, showing great potential for accelerating bone repair.[41] In this study, a novel SIM@HMSM/NP integrating a zwitterionic HMSM hydrogel with a 3D-printed NP scaffold was successfully developed for bone defect repair. The hydrogel component provided excellent biocompatibility, sustained drug release, and favorable water retention, while the NP scaffold offered mechanical stability and osteoconductivity. The incorporation of SIM further endowed the composite with osteoinductive and angiogenic properties, facilitating synergistic regulation of bone regeneration. *In vitro* analyses demonstrated that the SIM@HMSM/NP exhibited superior mechanical performance, controlled degradation, and sustained drug release, effectively promoting BMSC proliferation and osteogenic differentiation. In *in vivo* models, the SIM@HMSM/NP scaffold significantly enhanced new bone formation and collagen matrix deposition while simultaneously stimulating neovascularization within the defect area. These findings confirm that the integration of bioactive hydrogel and 3D-printed scaffold achieves a desirable balance between biodegradability, mechanical support, and biological activity.

Overall, this work provides a versatile strategy for the design of multifunctional scaffolds that enable osteogenic–angiogenic coupling and efficient bone defect repair. The SIM@HMSM/NP holds strong potential for future translational applications in bone tissue engineering and regenerative medicine.

Acknowledgments

None.

Funding

This study was supported by the Taishan Scholar Project of Shandong Province (No. tstp20250511).

Conflict of interest

The authors declare they have no competing interests.

Author contributions

Conceptualization: Jianyi Li; Yukun Du
Data curation: Yang Qu; Ya-nan Wang
Formal analysis: Yang Qu; Ya-nan Wang; Weiqing Kong; Xiaofan Du
Funding acquisition: Yongming Xi
Investigation: Yang Qu; Ya-nan Wang; Guanghui Gu
Methodology: Yang Qu; Ya-nan Wang
Project administration: Jianyi Li; Yukun Du
Supervision: Jianyi Li; Yukun Du; Guanghui Gu
Writing – original draft: Yang Qu; Ya-nan Wang
Writing – review & editing: Jianyi Li; Yukun Du
All authors have read and approved the final version of the manuscript.

Ethics approval and consent to participate

All animal procedures were reviewed and approved by the Laboratory Animal Management and Ethics Committee of Qingdao University (Approval No. 20220910) and conducted in accordance with the Guidelines for the Care and Use of Laboratory Animals (National Research Council, United States of America) and the Guidelines for the Ethical Review of Experimental Animals in the People's Republic of China (GB/T 35892-2018).

Consent for publication

Not applicable.

Availability of data

The data that support the findings of this study are available from the corresponding author upon reasonable request.

References

1. Xu JL, Bao G, Jia B, *et al*. An adaptive biodegradable zinc alloy with bidirectional regulation of bone homeostasis for treating fractures and aged bone defects. *Bioact Mater*. 2024;38:207-224. doi: 10.1016/j.bioactmat.2024.04.027
2. Kim J, Park S, Park JY, *et al*. Dual-phase blocks for regeneration of critical-sized bone defects. *Nano Today*. 2024;54:102120. doi: 10.1016/j.nantod.2023.102120
3. Lee J, Byun H, Madhurakkat Perikamana SK, Lee S, Shin H. Current advances in immunomodulatory biomaterials for bone regeneration. *Adv Healthc Mater*. 2019;8(4):e1801106. doi: 10.1002/adhm.201801106
4. Yuan B, Cheng Q, Zhao R, *et al*. Comparison of osteointegration property between PEKK and PEEK: effects of surface structure and chemistry. *Biomaterials*. 2018;170:116-126. doi: 10.1016/j.biomaterials.2018.04.014
5. Wang JC, Dou ZL, Xia L, Huang N. Metal-organic complex coating for enhanced corrosion control and biocompatibility on biodegradable magnesium alloy for orthopaedic implants. *J Mat Chem B*. 2024;12(23):5661-5677. doi: 10.1039/d4tb00347k
6. Hama R, Ulziibayar A, Reinhardt JW, Watanabe T, Kelly J, Shinoka T. Recent developments in biopolymer-based hydrogels for tissue engineering applications. *Biomolecules*. 2023;13(2):280. doi: 10.3390/biom13020280
7. Cao H, Duan L, Zhang Y, Cao J, Zhang K. Current hydrogel advances in physicochemical and biological response-driven biomedical application diversity. *Signal Transduct Target Ther*. 2021;6(1):426. doi: 10.1038/s41392-021-00830-x
8. Huang QT, Zou YJ, Arno MC, *et al*. Hydrogel scaffolds for differentiation of adipose-derived stem cells. *Chem Soc Rev*. 2017;46(20):6255-6275. doi: 10.1039/c6cs00052e
9. Gu GH, Cui ZC, Du XF, *et al*. Recent advances in biomacromolecule-reinforced 2D material (2DM) hydrogels: from interactions, synthesis, and functionalization to biomedical applications. *Adv Funct Mater*. 2024;34(48):8367. doi: 10.1002/adfm.202408367
10. Tzoumani I, Iatridi Z, Fidelli A, Krassa P, Kallitsis J, Bokias G. Room-temperature self-healable blends of waterborne polyurethanes with 2-hydroxyethyl methacrylate-based polymers. *Int J Mol Sci*. 2023;24(3):2575. doi: 10.3390/ijms24032575
11. He X, He S, Xiang G, *et al*. Precise lubrication and protection of cartilage damage by targeting hydrogel microsphere. *Adv Mater*. 2024;36(40):2405943. doi: 10.1002/adma.202405943
12. Rodzen K, O'Donnell E, Hasson F, *et al*. Advanced 3D printing of polyetherketoneketone hydroxyapatite composites via fused filament fabrication with increased interlayer connection. *Materials (Basel)*. 2024;17(13):3161. doi: 10.3390/ma17133161
13. Derby B. Printing and prototyping of tissues and scaffolds. *Science*. 2012;338(6109):92-926. doi: 10.1126/science.1226340
14. Shafiee A, Atala A. Printing technologies for medical applications. *Trends Mol Med*. 2016;22(3):254-265. doi: 10.1016/j.molmed.2016.01.003
15. Li JY, Li KK, Du YK, *et al*. Dual-nozzle 3D printed nano-hydroxyapatite scaffold loaded with vancomycin sustained-release microspheres for enhancing bone regeneration. *Int J Nanomedicine*. 2023;18:307-322. doi: 10.2147/IJN.S394366
16. Rajabi M, McConnell M, Cabral J, Ali MA. Chitosan hydrogels in 3D printing for biomedical applications. *Carbohydr Polym*. 2021;260:117768. doi: 10.1016/j.carbpol.2021.117768
17. Vijayavenkataraman S, Yan WC, Lu WF, Wang CH, Fuh JYH. 3D bioprinting of tissues and organs for regenerative medicine. *Adv Drug Deliv Rev*. 2018;132:296-332. doi: 10.1016/j.addr.2018.07.004
18. Mandrycky C, Wang ZJ, Kim K, Kim DH. 3D bioprinting for engineering complex tissues. *Biotechnol Adv*. 2016; 34(4):422-434. doi: 10.1016/j.biotechadv.2015.12.011
19. Anada T, Pan CC, Stahl AM, *et al*. Vascularized bone-mimetic hydrogel constructs by 3D bioprinting to promote osteogenesis and angiogenesis. *Int J Mol Sci*. 2019;20(5):1096. doi: 10.3390/ijms20051096
20. Duarte JA, de Barros ALB, Leite EA. The potential use of simvastatin for cancer treatment: a review. *Biomed Pharmacother*. 2021;141:111858. doi: 10.1016/j.biopha.2021.111858
21. Yao X, Xie R, Cao Y, *et al*. Simvastatin induced ferroptosis for triple-negative breast cancer therapy. *J Nanobiotechnol*. 2021;19(1):311. doi: 10.1186/s12951-021-01058-1
22. Sun TT, Huang J, Zhang W, *et al*. Simvastatin-hydroxyapatite coatings prevent biofilm formation and improve bone

formation in implant-associated infections. *Bioact Mater*. 2023;21:44-56.
doi: 10.1016/j.bioactmat.2022.07.028

23. Chiu KY, Huang JY, Su YH, Ou SF, Chen KK, Wang YH. A 3D-printed bioactive glass scaffold coated with sustained-release PLGA/simvastatin stimulates calvarial bone repair. *Mater Des*. 2024;241:112898.
doi: 10.1016/j.matdes.2024.112898

24. Dai BY, Li X, Xu JK, *et al*. Synergistic effects of magnesium ions and simvastatin on attenuation of high-fat diet-induced bone loss. *Bioact Mater*. 2021;6(8):2511-2522.
doi: 10.1016/j.bioactmat.2021.01.027

25. Chiu KY, Huang JY, Su YH, Ou SF, Chen KK, Wang YH. A 3D-printed bioactive glass scaffold coated with sustained-release PLGA/simvastatin stimulates calvarial bone repair. *Mater Des*. 2024;241:112898.
doi: 10.1016/j.matdes.2024.112898

26. Zhen J, Wan T, Sun G, Chen X, Zhang S. A ROS-responsive microsphere capsule encapsulated with NADPH oxidase 4 inhibitor ameliorates macrophage inflammation and ferroptosis. *Heliyon*. 2024;10(1):e23589.
doi: 10.1016/j.heliyon.2023.e23589

27. Liu XF, Gaihre B, Park S, *et al*. 3D-printed scaffolds with 2D hetero-nanostructures and immunomodulatory cytokines provide pro-healing microenvironment for enhanced bone regeneration. *Bioact Mater*. 2023;27:216-230.
doi: 10.1016/j.bioactmat.2023.03.021

28. Gu GH, Xu YY, He P, *et al*. Bioinspired composite hydrogels with osteogenic, angiogenic, and antioxidant properties for enhanced bone repair. *Small Struct*. 2025;6(4):2400462.
doi: 10.1002/sstr.202400462

29. Çetin D, Kahraman AS, Gümüsderelioglu M. Novel scaffolds based on poly(2-hydroxyethyl methacrylate) superporous hydrogels for bone tissue engineering. *J Biomater Sci Polym Ed*. 2011;22(9):1157-1178.
doi: 10.1163/092050610x501704

30. Moura D, Pereira AT, Ferreira HP, *et al*. Poly(2-hydroxyethyl methacrylate) hydrogels containing graphene-based materials for blood-contacting applications: from soft inert to strong degradable material. *Acta Biomater*. 2023;164:253-268.
doi: 10.1016/j.actbio.2023.04.031

31. Kim S, Shin BH, Yang C, *et al*. Development of poly(HEMA-Am) Polymer hydrogel filler for soft tissue reconstruction by facile polymerization. *Polymers*. 2018;10(7):772.
doi: 10.3390/polym10070772

32. Gao F, Xu ZY, Liang QF, *et al*. Direct 3D printing of high strength biohybrid gradient hydrogel scaffolds for efficient repair of osteochondral defect. *Adv Funct Mater*. 2018;28(13):1706644.
doi: 10.1002/adfm.201706644

33. Wang LL, Chen X, Wang XY, *et al*. Bio-inspired mineralized collagen scaffolds with precisely controlled gradients for the treatment of severe osteoarthritis in a male rabbit model. *Int J Biol Macromol*. 2025;300:139843.
doi: 10.1016/j.ijbiomac.2025.139843

34. Pathmanapan S, Periyathambi P, Anandasadagopan SK. Fibrin hydrogel incorporated with graphene oxide functionalized nanocomposite scaffolds for bone repair — in vitro and in vivo study. *Nanomed*. 2020;29:102251.
doi: 10.1016/j.nano.2020.102251

35. Xue X, Hu Y, Deng YH, Su JC. Recent advances in design of functional biocompatible hydrogels for bone tissue engineering. *Adv Funct Mater*. 2021;31(19):2009432.
doi: 10.1002/adfm.202009432

36. Zhou D, Yan X, Xiao L, Wang JL, Wei JC. Gold capped mesoporous bioactive glass guides bone regeneration via BMSCs recruitment and drug adaptive release. *Chem Eng J*. 2024;487:150546.
doi: 10.1016/j.cej.2024.150546

37. Jang HJ, Yoon JK. The role of vasculature and angiogenic strategies in bone regeneration. *Biomimetics*. 2024;9(2):75.
doi: 10.3390/biomimetics9020075

38. Schott NG, Friend NE, Stegemann JP. Coupling osteogenesis and vasculogenesis in engineered orthopedic tissues. *Tissue Eng Part B Rev*. 2021;27(3):199-214.
doi: 10.1089/ten.teb.2020.0132

39. Yu WL, Sun TW, Qi C, *et al*. Enhanced osteogenesis and angiogenesis by mesoporous hydroxyapatite microspheresderived simvastatin sustained release system for superior bone regeneration. *Sci Rep*. 2017;7:44129.
doi: 10.1038/srep44129

40. Saberi A, Kouhjani M, Mohammadi M, Hosta-Rigau L. Novel scaffold platforms for simultaneous induction osteogenesis and angiogenesis in bone tissue engineering: a cutting-edge approach. *J Nanobiotechnol*. 2023;21(1):351.
doi: 10.1186/s12951-023-02115-7

41. Pan Q, Zong Z, Li H, *et al*. Hydrogel design and applications for periodontitis therapy: a review. *Int J Biol Macromol*. 2025;284:137893.
doi: 10.1016/j.ijbiomac.2024.137893